# Locating a weak change using diffuse waves: Theoretical approach and inversion procedure

Vincent Rossetto, Ludovic Margerin, Thomas Planès, Eric Larose

## ▶ To cite this version:

HAL Id: hal-00563872

https://hal.archives-ouvertes.fr/hal-00563872

Submitted on 7 Feb 2011

# Locating a weak change using diffuse waves (LOCADIFF): theoretical approach and inversion procedure

Vincent Rossetto[*1,2], Ludovic Margerin [3,4],
Thomas Planès [1,5] and Éric Larose [1,5]

[1]Université Joseph Fourier, Grenoble - CNRS
[2]Laboratoire de Physique et Modélisation des Milieux Condensés,
BP 166 25, avenue des Martyrs - 38042 Grenoble CEDEX, France
[3] Université Paul Sabatier, Toulouse - CNRS
[4] Institut de Recherche en Astrophysique et Planétologie,
14, avenue Édouard Belin, 31400 Toulouse, France
[5] Institut des Sciences de la Terre, BP 53, 38041 Grenoble, France

February 7, 2011

**Abstract**

We describe a time-resolved monitoring technique for heterogeneous media. Our approach is based on the spatial variations of the cross-coherence of diffuse waves acquired at fixed positions but at different dates. The technique applies to all kind of waves, provided that waveforms can be acquired with a sampling frequency much larger than the wave frequency. To locate and characterize a weak change that occurred between successive acquisitions, we use a maximum likelihood approach combined with a diffusive propagation model. We characterize this technique, called LOCADIFF, with the aid of numerical simulations. In several illustrative examples, we show

[*]vincent.rossetto@grenoble.cnrs.fr

1

that the change can be located with a precision of a few wavelengths and that its effective scattering cross-section can be retrieved. We investigate how the accuracy and precision of the method depends on the number of source-receiver pairs, on the time window used to compute the cross-correlation and on the errors in the propagation model. Applications can be found in non-destructive testing, seismology, radar and sonar location.

# 1   Introduction

Waves constitute one of the primary tools to detect and locate temporal changes. If the waves do not interact with any other obstacle than the target, conventional imaging techniques based on geometrical considerations apply. A controlled pulse emitted into the medium is scattered by the target and the echos are recorded with a receiver. These techniques can be improved using several sources and detectors, and extended to locating several targets at the same time. As long as the typical propagation time in the medium is much smaller than the scattering mean free time, i.e. the average time between two scattering events, we are in the single scattering regime. In this case, the precision for detecting and locating a change is limited by the Fresnel zone $\sqrt{\lambda L}$, with $L$ the typical propagation distance in the medium and $\lambda$ the wavelength. Applications in every day life abound: they cover high-stake fields like ultrasonic medical imaging, non-destructive testing, seismic exploration, radar aircraft location or sonar.

This simple picture does not apply in heterogeneous media such as polycrystals, concrete, or volcanoes. Imaging these materials in a non-destructive way is an important issue for miscellaneous applications like monitoring temporal changes or the assessment of ageing and damage. In heterogeneous media, ray theory is not relevant because the scattering mean free time is much smaller than the typical record duration. A pulse emitted into the medium experiences numerous scattering events and the output signal recorded at large distance from the source displays complex details that depend on the interactions between the wave and each of the scatterers. Beyond a distance called the transport mean free path $\ell^\star$, the memory of the initial direction of propagation is lost. In this regime, the average energy distribution in the medium evolves as a diffusion process and it is relevant to describe wave propagation with probabilities.

The problem of locating an isolated change in a multiple scattering sample has received some attention in the past, particularly in optics. The space and time correlations of intensity in a speckle pattern probed by one or more receivers al-

low one to observe the diffusion of scatterers [20, 3]. On the one hand, diffusive wave spectroscopy [5] and its variants have become standard tools for investigating collective changes in the medium. On the other hand previous authors [18] have shown that a local perturbation within a collection of scatterers (the background) essentially acts as a dipole source of intensity. Intensity variations enable the detection and location of a crack from observations in transmission [11, 31], or more generally to locate an object with known characteristics [8, 30]. The weak sensitivity of the method has been illustrated by numerical studies [31]. Indeed, a large amount of ensemble or frequency averaging (typically 100 realizations) is required to distinguish the intensity fluctuation caused by the defect from the background speckle pattern. From a theoretical point of view, the weak sensitivity of methods based on intensity variations can be traced back to the cancellation of scattering diagrams that dominate the decorrelation of waveforms, a cancellation which is imposed by the optical theorem. This renders techniques based on intensity variations almost inapplicable to solid media because ensemble averaging is impractical. These points will be further illustrated below.

In acoustics, one can commonly record a large number of signals with perfect temporal and spatial precision, which is advantageous compared to optics. A pulse emitted into a heterogeneous medium gives rise to long time records with a pronounced *coda*, a term which refers to the arrivals following the ballistic pulse. Several techniques use the coda to retrieve information on the evolution of the medium. In seismology, the monitoring of temporal changes in the crust was initiated in the mid-80's, using repeating small earthquakes [21]. Later on the method was applied to volcanoes and revealed temporal changes of velocity prior to eruptions [23] or measure the effect of permanent damage [24]. Recent developments of this technique have been popularized under the term coda-wave interferometry (CWI) [28, 19]. The correlation of waveforms inspired other techniques, like diffuse acoustic wave spectroscopy (DAWS) [6]. Recently DAWS has been used in damage monitoring [17, 29] but a large range of other applications are possible [27]. For a broad review of applications of CWI in geophysics, we refer to [22]. In a number of previous experiments, changes of waveforms were characterized by a stretching of the coda and interpreted in terms of travel time variations. Such an approach allows the detection of weak changes, but gives little information concerning the location of the change [23, 16, 13, 4] In many applications, waveforms changes result in decorrelation of the signals with or without additional stretching. This renders the interpretation of a local change in terms of travel time fluctuations problematic. Also based on the concept of correlation, techniques have been developed to recover the Green's function in an open

3

medium based on the cross correlation of noise signals [9, 14, 32, 33, 12], These noise-based Green's functions can in turn be used in a passive image interferometry technique with applications in volcanology and fault monitoring [25, 34, 4]. Recently, Aubry and Derode [2] proposed an alternative technique based on the singular value decomposition of the propagator, but this technique is limited to a sufficiently strong extra scatterer.

In this article, we report on a different approach to locate a weak isolated change. Our technique, called LOCADIFF, uses the correlations computed along time windows in the late part of the records for several pairs of sources and receivers. We use a numerical model to compute the most likely position of the weak change, in terms of probability. The purpose of this article is to introduce the principles of this technique and discuss its properties. Although the technique applies to waves of all kind, use elastic and acoustic waves for illustrations, because their frequency range allows an easily accessible experimental use. Experimental tests and results have been already published separately in Ref. [15] and will not be detailed here. To introduce this work, we observe in a finite difference numerical simulation the correlation loss induced by a weak change between impulse responses (Section 2). Using the theory of multiple scattering [30], we derive an expression of the decorrelation induced by a weak change in Section 3. We then present the inversion technique, based on the maximum likelihood principle in Section 4 and its properties are thereafter investigated. We explore the implementation of boundary conditions in Section 5. Finally, we discuss the accuracy of the technique and possible improvements in Section 6.

## 2   Observations of correlation loss after a weak change

Under the denomination "weak change", we understand any local change of impedance contrast caused by either the apparition of a defect, or a local change in a physical quantity, which modifies the effective value of the scattering cross-section if one describes the medium in the multiple scattering frame. Such a weak change between two sets of acquisitions is made by removing a single scatterer from a numerical model of a multiple scattering medium.

It is already known that a weak change can be detected in a scattering medium because it slightly modifies the Green's functions. The amount of modification is usually quantified by measuring the cross-correlation between waveforms recorded at different times [21]. We illustrate the signal processing with the aid of numerical simulations of the wave equation in a medium containing a large

number of identical scatterers.

## 2.1  Numerical simulations of wave propagation

As a first investigation, we perform 2D numerical experiments of acoustic wave propagation in heterogeneous media [1]. Using a finite difference scheme, we solve the wave equation with absorbing boundary conditions; the dimension of the simulation grid is $50\lambda_0 \times 50\lambda_0$, with a spatial discretization step $\lambda_0/30$, where $\lambda_0$ is the central wavelength. Synthetic data are computed on a linear array of 9 receivers located at the center of the medium and 10 sources are randomly distributed over the grid. Sources and receivers are kept fixed throughout the experiments (see Fig. 1). To mimic a multiple scattering medium, 800 empty cavities of diameter $\lambda_0/3$ are randomly distributed over the grid. In the frequency band of interest the average scattering cross-section was numerically estimated as $\Sigma = 1.6\lambda_0$, along with the transport cross section $\Sigma^\star = 1.1\lambda_0$. Table 1 summarizes the physical properties of the simulated medium, including the number of scatterers (with density $n$), the transport mean free path $\ell^\star = \frac{1}{n\Sigma^\star}$, the diffusion constant $D = \frac{c\ell^\star}{2}$ and the Thouless time $\tau_D = \frac{R^2}{6D}$, where $R^2$ is the mean squared distance between sources and receivers. Note that these quantities are evaluated under the "independent scattering approximation", which assumes that the scattering events are all uncorrelated.

| Parameter | notation | value |
|---|---|---|
| Number of scatterers | | 800 |
| Transport mean free path | $\ell^\star$ | $2.8\lambda_0$ |
| | $k\ell^\star$ | 18 |
| Diffusion constant | $D$ | $1.4\,\lambda_0^2/T_0$ |
| Thouless time | $\tau_D$ | $68\,T_0$ |
| Coda decay time (leakage) | $\tau_\sigma$ | $240\,T_0$ |

Table 1: Physical parameters of the simulations in normalized units.

The signal $e(t)$ emitted by each source is a pulse with central frequency $f_0$ and a Gaussian envelope (100% bandwitdh at -6dB). Using source $i$ we record with

---

[1]The code named ACEL has been developed by M. Tanter, Institut Langevin, Paris France. More details in http://www.institut-langevin.espci.fr/Mickael-Tanter,143
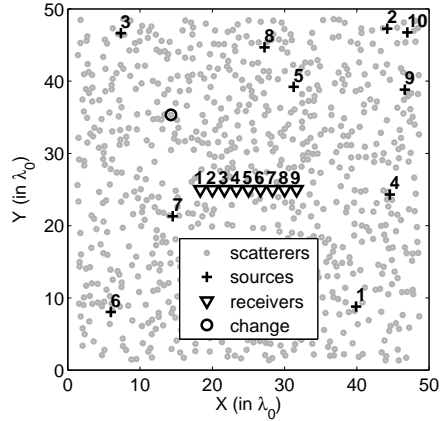
Figure 1: Distribution of sources, receivers, scatterers in the numerical simulation. The removed scatterer is indicated with a black circle.
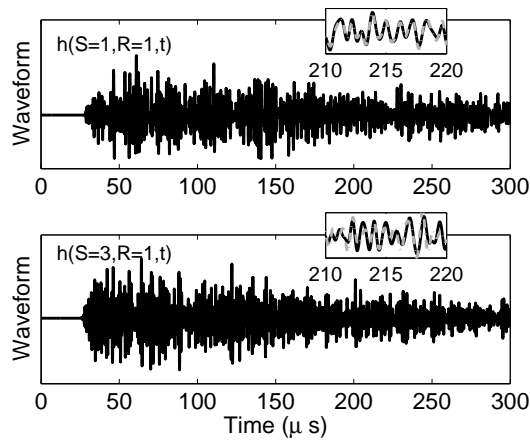


Figure 2: Normalized waveforms $h(t)$ obtained at receiver 1, for source number 1 (top) and 3 (bottom). Inset: zoom into the late waveforms. The black solid (resp gray broken) line corresponds to the record acquired before (resp. after) the change. For illustration purpose, the value of $T_0$ was set to $1\,\mu$s. The distance between receiver 1 and sources 1 and 3 are respectively $10.0\,\ell^\star$ and $9.0\,\ell^\star$.

receiver $j$ the signal $h_{ij}(t)$ during 300 oscillations of period $T_0$. Typical wave-forms $h_{ij}(t)$ are plotted in Fig. 2. The long tail of the record in Fig. 2 corresponds to arrival of partial waves that have been scattered several times. Notice that the ballistic arrival is not distinguishable in the waveforms of Figure 2. A long-lasting signal and the lack of ballistic arrival constitute evidences that we are in a strongly scattering regime, in agreement with our estimates of the transport mean free path. During the first run of the simulation, $10 \times 9$ impulse responses $h_{ij}$ are recorded and stored. On a second run, one scatterer is removed and another set of impulse responses $h'_{ij}$ is evaluated. Both $h_{ij}(t)$ and $h'_{ij}(t)$ display signals lasting a large number of ballistic times.

## 2.2   Detection of a weak change

The details of the complex waveforms shown in Figure 2 are highly sensitive to the positions of the scatterers. Each waveform can be understood as a fingerprint of the medium. As our goal is to detect a single scatterer's removal, we need to exploit the information contained in both the amplitude and phase of the signals. A comparison between the records $h_{ij}(t)$ and $h'_{ij}(t)$ reveals that for short times up to $100\,T_0 \approx 30\tau^*$, no difference is visible in the signals. We observe small differences between the waveforms at later times that are solely due to the change in the medium. Figure 2 (bottom) shows a comparison of the waveforms between $h_{3,1}(t)$ and $h'_{3,1}(t)$ in the time window $t \in [210\,T_0, 220\,T_0]$. The observed decorrelation is too large to be attributed to numerical noise, there is thus evidence that the waveforms are sensitive to the removal of only one scatterer.

The differences between the waveforms $h_{ij}$ and $h'_{ij}$ are quantified by the decorrelation, or correlation loss, between $h_{ij}$ and $h'_{ij}$. The decorrelation is computed on a time window of duration $2T$ centered on $t$ using the formula:

$$K_{ij}(t) = 1 - \frac{\int_{t-T}^{t+T} h_{ij}(u)\,h'_{ij}(u)\mathrm{d}u}{\sqrt{\int_{t-T}^{t+T} h_{ij}(u)^2\mathrm{d}u \int_{t-T}^{t+T} h'_{ij}(u')^2\mathrm{d}u'}}. \tag{1}$$

The typical width of the time window $T$ is of order $5T_0$. Experimentally, enlarging $T$ partly eliminates the effect of noise and reduces the fluctuations of the correlation coefficient. However, using a large value for $T$ results in considering simultaneously paths with very different lengths. We address this important point in Section 3.2.

## 2.3 Spatial dependence of the decorrelation

In Figure 2, it is noticeable that the differences between $h_{1,1}$ and $h'_{1,1}$ (top), are much smaller than the differences between $h_{3,1}$ and $h'_{3,1}$ (bottom), even in the late signal. The decorrelations computed over the interval $[210\,T_0,\ 220\,T_0]$ ($t = 215\,T_0$) are $K_{1,1}(t) = 5\%$ and $K_{3,1}(t) = 27\%$, respectively. Consequently, the amount of decorrelation depends on the positions of the source and receiver with respect to the local change, a property which holds even in very late time windows in the signal. For a given configuration of source-receiver pairs, we obtain a set of observed decorrelations, which is characteristic of the relative locations of the sources and receivers to the change in the multiple scattering medium. We will now demonstrate the possibility to locate the change and estimate its cross-section from the knowledge of the source and receiver positions and the corresponding decorrelation coefficients. To do so, we develop a theoretical model to predict the decorrelation coefficient of waves induced by the addition of a change in a heterogeneous medium, in the diffusive regime. We recall in the next section the necessary elements from multiple scattering theory.

# 3 Wave scattering theory

We assume that the medium can be represented as a uniform background with embedded inclusions. Only the scalar case is considered here. The scattering properties of an inclusion will be described by its $\mathcal{T}$ matrix, defined in operator notation as [26, 10]:

$$G_1 = G_0 + G_0 \mathcal{T} G_0 \qquad (2)$$

where $G_0$ is the retarded free space Green's function and $G_1$ is the Green's function in the presence of the scatterer. For a non absorbing scatterer, energy conservation implies the following optical theorem:

$$-\frac{\Im \mathcal{T}(\omega)}{k_0} = \sigma(\omega), \qquad (3)$$

where $\sigma$ is the scatterer cross-section.

## 3.1 Correlations between two slightly different media

We want to predict the decorrelation of waveforms in a medium where a weak change occurs. Although we will employ a statistical approach based on ensemble

averages, in general we have access to only one realization of the random process. Therefore we introduce the following estimator of the cross-correlation function based on the observation of a single diffuse signal:

$$\Gamma(t,\,\tau) = \frac{1}{2T} \int_{t-T}^{t+T} \psi^2(t' + \tau/2)\psi^1(t' - \tau/2)\mathrm{d}t', \qquad (4)$$

where $\psi$ is the scalar field. The superscript 2 refers to the medium in presence of change while the superscript 1 refers to the medium without it. We have introduced an analog of the Wigner function which is most convenient to analyze non-stationary signals. The empirical cross-correlation can be decomposed into internal and external frequencies $\omega$ and $\Omega$, respectively:

$$\Gamma(t,\,\tau) = \frac{1}{(2\pi)^2} \int_{-\infty}^{\infty} \mathrm{d}\Omega \int_{-\infty}^{\infty} \mathrm{d}\omega \tilde{\Gamma}(\Omega,\,\omega) \, \exp[-\mathrm{i}(\Omega t + \omega\tau)] \qquad (5)$$

where the frequency-domain cross-correlation reads:

$$\tilde{\Gamma}(\Omega,\,\omega) = \mathrm{sinc}(\Omega T)\,\psi^2(\omega + \Omega/2)\psi^1(\omega - \Omega/2)^*. \qquad (6)$$

The frequency $\Omega \ll \omega$ describes the slow envelope of diffuse waves with central frequency $\omega$. Equation (6) shows that basic quantity to be computed is

$$\left\langle G^2(\omega + \Omega/2)G^1(\omega - \Omega/2)^* \right\rangle, \qquad (7)$$

where $G$ is the retarded Green's function. We will denote by $\mathcal{T}_0$ the $\mathcal{T}$-matrix of the change which is assumed to appear at the position $\mathbf{x}_0$. In diagrammatic notations, such as the one employed in Figure 3, the $\mathcal{T}$ matrices are represented by crosses. The transport of energy in the scattering medium is described by the ladder propagator $L$, which is defined by the diagrammatic self-consistent equation shown in Figure 3 [26, 1].

We use the field-field correlation function in the diffuse signal

$$\tilde{\Gamma}(\omega,\,\Omega,\,\mathbf{s},\,\mathbf{x}_0,\,\mathbf{r}) = \int \mathrm{d}\mathbf{r}_1 \int \mathrm{d}\mathbf{r}_2 \, \tilde{P}_0(\omega,\,\Omega,\,\mathbf{s},\,\mathbf{r}_1)\tilde{L}_e(\omega,\,\Omega,\,\mathbf{r}_1,\,\mathbf{x}_0,\,\mathbf{r}_2)\tilde{P}_0(\omega,\,\Omega,\,\mathbf{r}_2,\,\mathbf{r}).$$
$$(8)$$

Quantities labelled with ˜ are implicitly evaluated at inner frequency $\omega$ and outer frequency $\Omega$. $L_e$ is the correlation between between the wavefields recorded before and after the change occured. $\tilde{P}_0(\mathbf{s},\,\mathbf{r}_1)$ and $\tilde{P}_0(\mathbf{r}_2,\,\mathbf{r})$ describe the ballistic
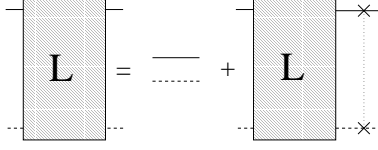
Figure 3: The Bethe-Salpeter equation defining the so-called ladder operator $L$. The solid line and dashed line represent the retarded ensemble averaged Green's function and its complex conjugate, respectively. The dotted line connecting the two vertices indicates that they represent the same scatterer.

propagation from the source to the first scattering event, and from the last scattering event to the detector, respectively:

$$\tilde{P}_0(\mathbf{r}_1,\ \mathbf{r}_2) = \frac{e^{-R/\ell}}{(4\pi R)^2}\, e^{i\Omega R/c} \tag{9}$$

where $R = |\mathbf{r}_2 - \mathbf{r}_1|$ and $c = \partial_\omega k_0(\omega)$ is the group velocity at the frequency $\omega$. The ladder propagator with the extra-scatterer $L_e$ is related to the ladder propagator without the extra-scatterer $L$ as follows [18]:
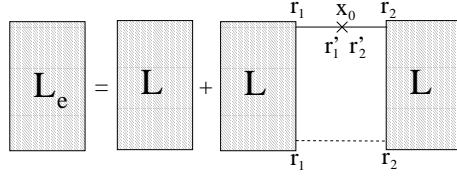


Figure 4: The diagram of the ladder operator with an extra scatterer. The extra scatterer is sandwiched between two ladder operators. Note that we have neglected the possibility that ensemble averaged Green's functions connect the extra scatterer with the source and/or the receiver which assumes that it is located at least one mean free path away from all sources and receivers. Locating the change if it occurs next to the source or the receiver is still possible, but would require to slightly modify the theory.

$$\tilde{L}_e(\mathbf{s},\ \mathbf{x}_0,\ \mathbf{r}) = \tilde{L}(\mathbf{s},\ \mathbf{r}) + \int d\mathbf{r}_1 \int d\mathbf{r}_2 \tilde{L}(\mathbf{s},\ \mathbf{r}_1)\tilde{J}(\mathbf{r}_1,\ \mathbf{x}_0,\ \mathbf{r}_2)\tilde{L}(\mathbf{r}_2,\ \mathbf{r}). \tag{10}$$

In Equation (10), also represented by the diagram depicted in Figure 4, the first term represents the scattering paths that do not see the change, while the second

10

term describes the paths that visit the change once. As we are in a regime of weak interaction between the field and the scatterer, higher-order terms can be neglected. Note that this is consistent with the fact that such terms are neglected in the ladder approximation adopted in this work. We define the operator $J$ that connects the two ladders by

$$\tilde{J}(\mathbf{r}_1,\,\mathbf{x}_0,\,\mathbf{r}_2) = \int \mathrm{d}\mathbf{r}_1' \int \mathrm{d}\mathbf{r}_2'\, \tilde{G}(\mathbf{r}_1,\,\mathbf{r}_1')\tilde{\mathcal{T}}(\mathbf{r}_1',\,\mathbf{r}_2')\tilde{G}(\mathbf{r}_2',\,\mathbf{r}_2)\tilde{G}(\mathbf{r}_1,\,\mathbf{r}_2)^*, \qquad (11)$$

where $G$ denotes the ensemble averaged Green's function. For a point scatterer in the mesoscopic regime, as the variations of the envelope are slow, we evaluate $J$ to the lowest order of the small quantity $1/(k_0\ell) \ll 1$ [30]

$$\tilde{J}(\mathbf{r}_1,\,\mathbf{x}_0,\,\mathbf{r}_2) \simeq -\frac{\mathrm{i}\ell^2\mathcal{T}_0}{8\pi k_0}\delta^{(3)}(\mathbf{r}_1 - \mathbf{x}_0)\delta^{(3)}(\mathbf{x}_0 - \mathbf{r}_2). \qquad (12)$$

Inserting expression (12) into equation (8) one obtains:

$$\tilde{\Gamma}(\mathbf{s},\,\mathbf{x}_0,\,\mathbf{r}) = \int \mathrm{d}\mathbf{r}_1 \int \mathrm{d}\mathbf{r}_2 \tilde{P}_0(\mathbf{s},\,\mathbf{r}_1)\tilde{L}(\mathbf{r}_1,\,\mathbf{r}_2)\tilde{P}_0(\mathbf{r}_2,\,\mathbf{r})$$
$$- \int \mathrm{d}\mathbf{r}_1 \int \mathrm{d}\mathbf{r}_2 \tilde{P}_0(\mathbf{s},\,\mathbf{r}_1)\tilde{L}(\mathbf{r}_1,\,\mathbf{x}_0)\frac{\mathrm{i}\ell^2\mathcal{T}_0}{8\pi k}\tilde{L}(\mathbf{x}_0,\,\mathbf{r}_2)\tilde{P}_0(\mathbf{r}_2,\,\mathbf{r}), \quad (13)$$

where the first term is the diffuse intensity in the medium without extra scatterer and the second integral is an interference term caused by the extra scatterer. In the slowly-varying envelope approximation, the integrals can be evaluated to give:

$$\tilde{\Gamma}(\mathbf{s},\,\mathbf{x}_0,\,\mathbf{r}) = \frac{\ell^2}{4\pi^2}\tilde{L}(\mathbf{s},\,\mathbf{r}) - \frac{\ell^2}{4\pi^2}\tilde{L}(\mathbf{s},\,\mathbf{x}_0)\frac{\mathrm{i}\ell^2\mathcal{T}_0}{8\pi k_0}\tilde{L}(\mathbf{x}_0,\,\mathbf{r}). \qquad (14)$$

In the diffusive regime, the propagator of the wave intensity in the multiple scattering medium, $\tilde{P}_d$, is the solution of the following diffusion equation

$$\left(-\mathrm{i}\Omega - D\nabla_{\mathbf{r}_2}^2\right)\tilde{P}_d(\mathbf{r}_1,\,\mathbf{r}_2) = \delta^{(3)}(\mathbf{r}_1 - \mathbf{r}_2), \qquad (15)$$

where $D$ is the diffusivity. The ladder $L$ is related to $P_d$ by $\tilde{L}(\mathbf{r}_1,\,\mathbf{r}_2) = \frac{4\pi c}{\ell^2}\tilde{P}_d(\mathbf{r}_1,\,\mathbf{r}_2)$. Using these notations the correlation function between wavefields before and after the change can be rewritten as:

$$\tilde{\Gamma}(\mathbf{s},\,\mathbf{x}_0,\,\mathbf{r}) = \frac{c}{4\pi}\tilde{P}_d(\mathbf{s},\,\mathbf{r}) + \frac{c}{4\pi}\tilde{P}_d(\mathbf{s},\,\mathbf{x}_0)\frac{\mathrm{i}c\mathcal{T}_0}{2k_0}\tilde{P}_d(\mathbf{x}_0,\,\mathbf{r}). \qquad (16)$$

In order to obtain the correlation function in the time domain, we double invert the Fourier transform over the variables $\omega$ and $\Omega$. We further assume that the signal has been filtered in a narrow frequency band $\Delta\omega$ in which the scattering properties vary little. Upon integration over $\omega$ and application of the optical theorem (3), the correlation function for a unit point-source normalized by the bandwidth $\Delta\omega$ reads:

$$\Gamma(\mathbf{s},\, \mathbf{x}_0,\, \mathbf{r},\, t) = P_d(\mathbf{s},\, \mathbf{r},\, t) - \frac{c\sigma}{2} \int_0^t \mathrm{d}u\, P_d(\mathbf{s},\, \mathbf{x}_0,\, u)P_d(\mathbf{x}_0,\, \mathbf{r},\, t - u). \quad (17)$$

We have therefore obtained the theoretical decorrelation $K(\mathbf{x}_0, t) = \frac{c\sigma}{2}Q(\mathbf{s},\, \mathbf{x}_0,\, \mathbf{r},\, t)$, where

$$Q(\mathbf{s},\, \mathbf{x}_0,\, \mathbf{r},\, t) = \frac{\int_0^t \mathrm{d}u\, P_d(\mathbf{s},\, \mathbf{x}_0,\, u)P_d(\mathbf{x}_0,\, \mathbf{r},\, t - u)}{P_d(\mathbf{s},\, \mathbf{r},\, t)}. \quad (18)$$

The negative sign in (17) comes from the optical theorem (energy conservation) and ensures that the cross-coherence is less than one. For a resonant point scatterer, $\sigma$ can be substituted with $\lambda_0^2/\pi$. The derivation presented in this section does not depend on the form of Equation (15) as long the envelope is slowly varying, which means that solutions to a more accurate transport equation can be substituted to $P_d$.

## 3.2 Computation of the decorrelation formula

We observe that the decorrelation (18) can be computed if the function $P_d$ is known. In the general case where the diffusivity $D$ depends on the position, the function $P_d$ can only be numerically estimated, provided that the spatial dependence of $D$ is known. In practice, the decorrelation coefficient can be reasonably rapidly computed if one assumes that the value of $D$ is approximately uniform in the medium. We investigate the acceptable amount of spatial variation of $D$ in Section 4.5.

If the medium is absorbing, the same issue arises. In media with a uniform absorption time $\kappa^{-1}$, the absorption affects the numerator of $Q$ in (18) by a factor $\exp[-\kappa u - \kappa(t - u)] = \exp[-\kappa t]$ and the denominator by a factor $\exp[-\kappa t]$. Therefore, uniform absorption effects cancel out in the normalized decorrelation function, which is a genuine advantage of the present technique. In the case where absorption is non-uniform, it will affect differently $P_d(\mathbf{s},\, \mathbf{x}_0)$ and $P_d(\mathbf{x}_0,\, \mathbf{r})$ and the observed decorrelation pattern may be partly ascribed to the spatial variations of absorption. Consider a medium with constant diffusivity $D$ and absorption $\kappa$.

The solution of the diffusion equation (15) in an infinite $d$-dimensional medium is

$$P_d(\mathbf{r}_1,\,\mathbf{r}_2,\,t) = \frac{1}{(4\pi Dt)^{d/2}} \exp\left[-\kappa t - \frac{(\mathbf{r}_2 - \mathbf{r}_1)^2}{4Dt}\right]. \tag{19}$$

In the case of a 3-D infinite medium, a usual Laplace transform calculation gives the exact result:

$$Q(\mathbf{s},\,\mathbf{x},\,\mathbf{r},\,t) = \frac{1}{4\pi D}\left(\frac{1}{s} + \frac{1}{r}\right)\exp\left[\frac{R^2 - (s+r)^2}{4Dt}\right]. \tag{20}$$

where we have introduce the notations $s = \|\mathbf{s}-\mathbf{x}\|$, $r = \|\mathbf{r}-\mathbf{x}\|$ and $R = \|\mathbf{s}-\mathbf{r}\|$. We observe that $Q$ is a function with elliptic contour lines multiplied by simple poles located at $\mathbf{s}$ and $\mathbf{r}$. Of course, if $\mathbf{r} = \mathbf{s}$, we recover the formula derived in Ref. [28] for an infinite medium. This formula is generally not applicable under this form because the transducers are usually located at the surface of the system. However, if the boundary conditions are sufficiently simple, the formula (20) can be used as a building block to derive more complicated solutions, as shown in Section 5.

In formula (17) we neglect two constraints. First, we assume that the change occurs at a minimum distance of the order of one mean free path from the source and the receiver. Second, we neglect the finite velocity of the wave, in other words, the contribution for times $u, t - u < R/c$ in the integral (17) should be removed. The contribution of short times $u < R/c$ in (17) is negligible as soon as $ct \gg R > \ell^\star$. The computation of the decorrelation coefficients $K_{ij}(t)$ must be done with $T$ larger than a few oscillation periods of the wave. Using formula (20), we can estimate the correction due to this averaging as a function of $T/t$. To do so, we compute the average of (20) on the interval $[t - T,\, t + T]$ and divide by the value of $Q$ at $t$. We obtain a curve of relative correction as a function of $T/t$ which is independent of any other parameters and which is displayed on Figure 5. In most applications, the correction will be typically less than 10%.

## 3.3 Intensity variations vs field correlations

As recalled in the introduction, a number of investigations on the monitoring of complex media have focused on the detection of intensity variations induced by local changes of the scattering properties. We will show that in the diffusive regime, intensity variations are much less sensitive to local changes than field correlations. To do so, we calculate the perturbation of the ladder propagator induced by
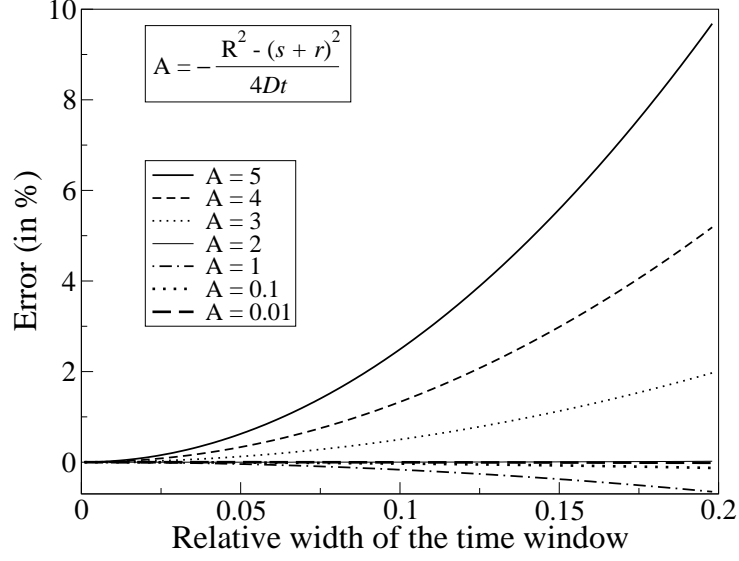
Figure 5: Deviation of the average of $Q$ on the time interval $[t - T, \, t + T]$ with repect to $Q(t)$. The correction grows more rapidly for large values of the argument in the exponential of (20), denoted by A in this Figure.

an extra-scatterer following the approach developed in reference [18]. In addition to the diagram depicted in Figure 4, two other diagrams contribute to intensity variations: 1) a diagram with a single cross on the lower line and 2) a diagram with one cross on each line which are connected by a dotted line. In the diffusive regime and for a non-absorbing change, we obtain the intensity perturbation to lowest-order in the small parameter $1/k_0\ell$ in the form:

$$\delta L_e^I(\mathbf{s}, \, \mathbf{x}, \, \mathbf{r}; \, t) = \frac{\ell^4 \mathcal{T}_0 \mathcal{T}_0^\star}{48\pi^2} \int_{-\infty}^{+\infty} \frac{\mathrm{d}\Omega}{2\pi} \iiint_{\mathbb{R}^3 \times \mathbb{R}^3} \mathrm{d}^3\mathbf{q} \, \mathrm{d}^3\mathbf{q}'$$
$$\tilde{L}(\mathbf{q}; \Omega) \mathrm{e}^{\mathrm{i}\mathbf{q}\cdot(\mathbf{r}-\mathbf{x})} (\mathbf{q} \cdot \mathbf{q}') \tilde{L}(\mathbf{q}'; \Omega) \mathrm{e}^{\mathrm{i}\mathbf{q}'\cdot(\mathbf{x}-\mathbf{s})} \mathrm{e}^{-\mathrm{i}\Omega t}. \quad (21)$$

In the Fourier domain, the ladder propagator in the diffusion regime writes:

$$\tilde{L}(\mathbf{q}; \Omega) = \frac{4\pi}{(2\pi)^3 \ell^2 \, (q^2\ell/3 - \mathrm{i}\Omega/c)}. \quad (22)$$

After integration over the wavenumbers $\mathbf{q}$, $\mathbf{q}'$ and the frequency $\Omega$, we obtain:

$$\delta L_e^I(\mathbf{s}, \, \mathbf{x}, \, \mathbf{r}; \, t) = \frac{\sigma c}{6\pi^{1/2}(Dt)^{3/2}} \mathrm{e}^{-R^2/4Dt} \nabla_{\mathbf{s}} \cdot \, (\nabla_{\mathbf{r}} Q(\mathbf{s}, \, \mathbf{x}, \, \mathbf{r})). \quad (23)$$

14

After calculation of the partial derivatives, we obtain the following formula for the ladder perturbation induced by an extra scatterer:

$$\delta L_e^I(\mathbf{s},\,\mathbf{x},\,\mathbf{r};t) = \frac{\sigma c^2 (\mathbf{r}-\mathbf{x})\cdot(\mathbf{s}-\mathbf{x})}{48\pi^{3/2} D^{7/2} t^{5/2} r^2 s^2} \left( \frac{r^3+s^3}{rs} + \frac{(r+s)^3}{2Dt} \right) e^{-(r+s)^2/4Dt}$$

(24)

The intensity variation exhibits a characteristic pattern with positive and negative lobes, depending on the cosine of the angle between the source and receiver as seen from the additional scatterer. Even more important is the temporal dependence $t^{-5/2}$ which is faster than the temporal decay of the ladder propagator between the source and receiver. As a consequence, the sensitivity to the local change decays like $1/t$ in sharp contrast to the field correlation which goes to a constant at large record time. This property supports the use of field correlation functions to monitor temporal changes in evolving media.

# 4  The inversion procedure

## 4.1  Maximum likelihood of the position

In Section 3, we have obtained an expression for the expected decorrelation as a function of the position of the change. The principle of the inversion procedure is to compare a theoretical model to the experimental data. The change is found at the position where numerical and experimental decorrelation match best. The mismatch is measured by a standard least-squares cost function ($\chi^2$). The inversion procedure consists in finding the position $\mathbf{x}$ and the cross-section $\sigma$ minimizing the function $\chi^2$. Such a technique is also often called a maximum likelihood method. Let us chose a set of sources $\mathbf{s}_i$ ($1 \leq i \leq n_s$) and a set of receivers $\mathbf{r}_j$ ($1 \leq j \leq n_r$), and call $N$ the number of source-receiver pairs (in this case, $N = n_r n_s$). There is no restriction on their positions, and in particular source and receiver can be located at the same position. We describe the technique at fixed time $t$ in the signal.

The most restrictive assumption of our approach is that a single change affects the experimental values of the decorrelation. The LOCADIFF inversion procedure consists in retrieving the most likely position of this change by introducing the cost function:

$$e(\mathbf{x}) = \sum_{i,j} \left( K_{ij}^m(t) - K_{ij}(\mathbf{x},\,t) \right)^2 / \epsilon^2,$$
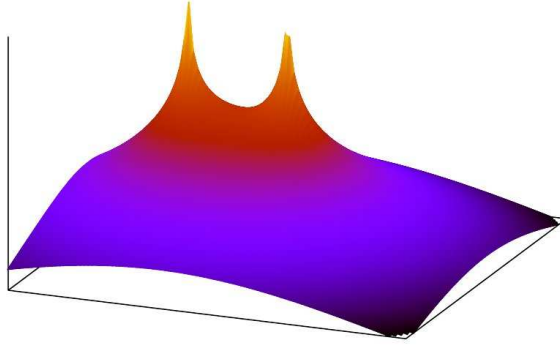
(25)

15

Figure 6: The function $Q_{ij}(\mathbf{x})$ in a infinite medium in dimension 3 with constant diffusivity and absorption computed with formula (20). The function is plotted in the plan containing the source, the receiver and the change. The value along the $z$ axis (logarithmic) is the sensitivity to a change at the position in $(x, y)$. The two peaks correspond to the positions of the source and the receiver. The $z$-scale is logarithmic and arbitrary.

where $K_{ij}^m(t)$ denotes the experimental measurements of the decorrelation and the coefficients $K_{ij}(\mathbf{x}, t)$ are the theoretical decorrelations assuming that the change is located at $\mathbf{x}$. The typical fluctuations on the measured decorrelations are encapsulated in the parameter $\epsilon$.

To find the value of the scattering cross-section $\sigma$, also unknown, we remark that $e(\mathbf{x})$ is, as a function of $\sigma$, a polynomial of degree two. There is therefore a minimum depending on $\mathbf{x}$ at

$$\sigma_{\text{opt}}(\mathbf{x}) = \frac{2}{c} \frac{\sum_{i,j} K_{ij}^m(t) Q_{ij}(\mathbf{x}, t)}{\sum_{i,j} Q_{ij}(\mathbf{x}, t)^2}. \tag{26}$$

We reintroduce the value of $\sigma_{\text{opt}}$ into the expression (25) and get the optimized error function

$$e_{\text{opt}}(\mathbf{x}) = \sum_{i,j} \frac{K_{ij}^m(t)^2}{\epsilon^2} - \frac{\left( \sum_{i,j} K_{ij}^m(t) Q_{ij}(\mathbf{x}, t) \right)^2}{\epsilon^2 \sum_{i,j} Q_{ij}(\mathbf{x}, t)^2} \tag{27}$$

which does not depend on $\sigma$ anymore. The most likely position of the change is the position $\mathbf{x}_0$ of the minimum of $e_{\text{opt}}$. The value of the cross-section is $\sigma_{\text{opt}}(\mathbf{x}_0)$ obtained from Equation (26).

16

To give an interpretation to the values of $e(\mathbf{x})$, it is customary to normalize it in the following way

$$\chi_n^2(\mathbf{x}) = \frac{e(\mathbf{x})}{f} \tag{28}$$

where $f = N - 4$ is the number of degrees of freedom, since four model parameters — the cross-section and the cartesian coordinates of the change — are to be estimated. The quantity $\chi_n^2(\mathbf{x})$ has the following interpretations. If $\chi_n^2(\mathbf{x}) \gg 1$, it is very unlikely that the point $\mathbf{x}_0$ is actually located at $\mathbf{x}$. If $\chi_n^2(\mathbf{x}) \simeq 1$ the point $\mathbf{x}$ is a good candidate for $\mathbf{x}_0$. If $\chi_n^2(\mathbf{x}_0) \ll 1$, there is a large area where $\chi_n^2(\mathbf{x}) < 1$ which means that the inversion could not locate precisely the change probably because the value of $\epsilon$ is too large. A large value of $\epsilon$ means either that the quality of measurements is poor or that $\epsilon$ has been overestimated. It is possible to use $\chi_n^2(\mathbf{x})$ to obtain the probability density that the change has occured at the point $\mathbf{x}$, which we define as:

$$p(\mathbf{x}) = \frac{1}{C} \exp\left[ -\frac{1}{2} f \chi_n^2(\mathbf{x}) \right] = \frac{1}{C} \exp\left[ -\frac{e(\mathbf{x})}{2} \right] \tag{29}$$

where $C$ is a normalization constant such that $\int p(\mathbf{x}) \mathrm{d}\mathbf{x} = 1$ (see the appendix for a derivation of this formula).

## 4.2   Precision versus number of source-receiver pairs

To investigate the precision of the inversion procedure depending on the parameters of the likelihood maximization, we use a numerical approach. We compute the best achievable precision regardless of all experimental difficulties that potentially degrade the accuracy of the location. We use an ideal set-up made of one source and $N$ receivers regularly distributed on a circle (see figure 8). We introduce a change at the center of the circle by adding a single scatterer with cross-section $\sigma$. For each pair of receiver, we compute synthetic data through application of the formula (20). The Thouless time $\tau_D$ is defined as $L^2/D$. As a measure of the precision, the length $\delta$ is introduced, which we compute using the probability density function (29) as follows: $\delta^2 = \int (\mathbf{x} - \mathbf{x}_0)^2 p(\mathbf{x}) \mathrm{d}\mathbf{x}$.

In the vicinity of the change, we infer that the contributions of the terms in $e(\mathbf{x})$ are comparable and we deduce that $\delta \propto \epsilon$. Thus, the precision with which the measurements are made directly influences the precision with which the change is located. We will not study the dependence of $\delta$ with respect to $\epsilon$ and we chose a value $\epsilon = 0.01$ throughout the numerical study. Note that a uniform probability distribution corresponds to a complete absence of information concerning
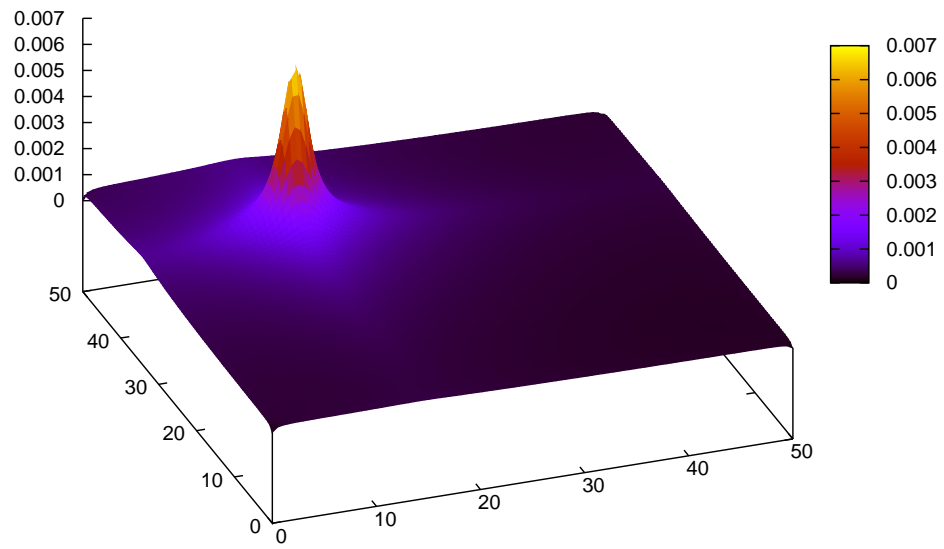
17

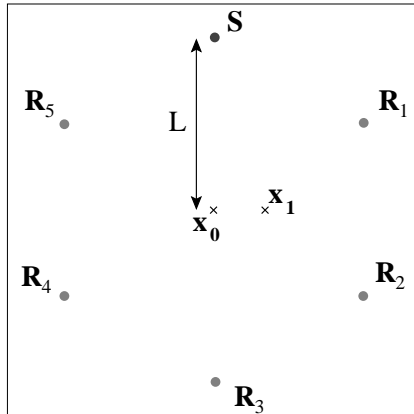Figure 7: Density of probability for the position of the moving scatterer.

Figure 8: Description of the numerical setup used for investigating the accuracy of the inversion procedure. The example is shown with $N = 5$. The other parameters of the numerical simulations are : $L = 10$, $D = 1$, $c = 1$. The change $\mathbf{x}_0$ is located at the center of the circle and is used in Section 4.2 to study the optimal spatial precision of the inversion. The change located at point $\mathbf{x}_1$ is used to study the robustness of the inversion procedure against measurement errors on the determination of $D$ in Section 4.5.

the location of the change, and gives the value $\delta \simeq L$. The typical behaviour of the precision $\delta$ as a function of the number of source-receiver pairs is depicted in Figure 9. In the configuration described above, each pair gives a comparable contribution to $e(\mathbf{x})$ so that $e(\mathbf{x})$ is approximately proportional to $N$. Therefore in the ideal case described in our example, we find that $\delta \propto N^{-1/2}$.

Note that the precision cannot be made arbitrarily small by increasing $N$ at will, because it is not possible to find an arbitrary number of source-receiver pairs providing *independent* data. The value $N$ entering into the scaling law $\delta \propto N^{-1/2}$ is the number of independent decorrelation measurements. Typically, in the diffusive regime, two measurements located $\lambda$ apart can be considered as independent.

## 4.3 Precision versus record time

The dependence of the precision $\delta$ with respect to record time is shown on Figure 10 for $\sigma = 1$, $D = 1$, $c = 1$, $L = 10$ and $\epsilon = 0.01$ (the units are dimensionless in the numerical simulation). The precision exhibits a minimum at a time of order $t_{\min} = \tau_D$. For a given source-receiver pair, the record time is the time that has elapsed after the arrival of the ballistic wave. Shortly after the ballistic arrival, the
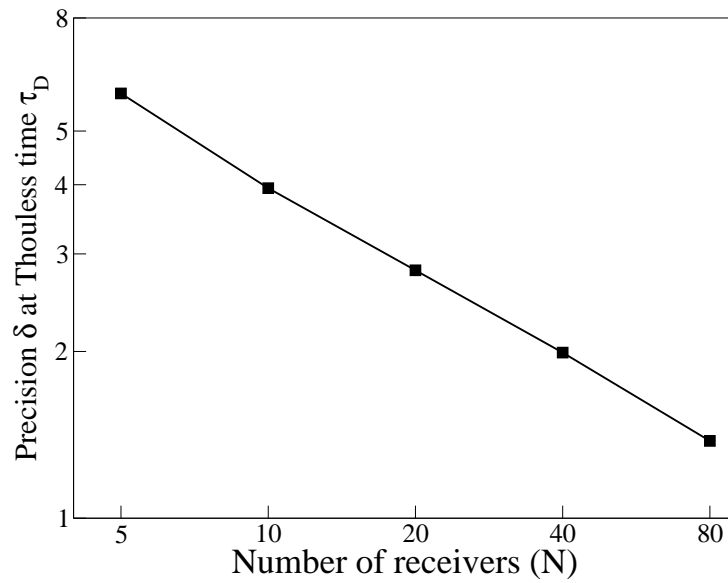
Figure 9: Spatial precision at the record time $t = \tau_D$, as a function of the number of receivers, where $\tau_D$ is the Thouless time. The typical setup for the numerical experiment is depicted in Figure 8. The dots correspond to the values of the precision for $N = 5, 10, 20, 40$ and $80$. The double logarithmic scale provides clear evidence of the relation $\delta \sim N^{-1/2}$.
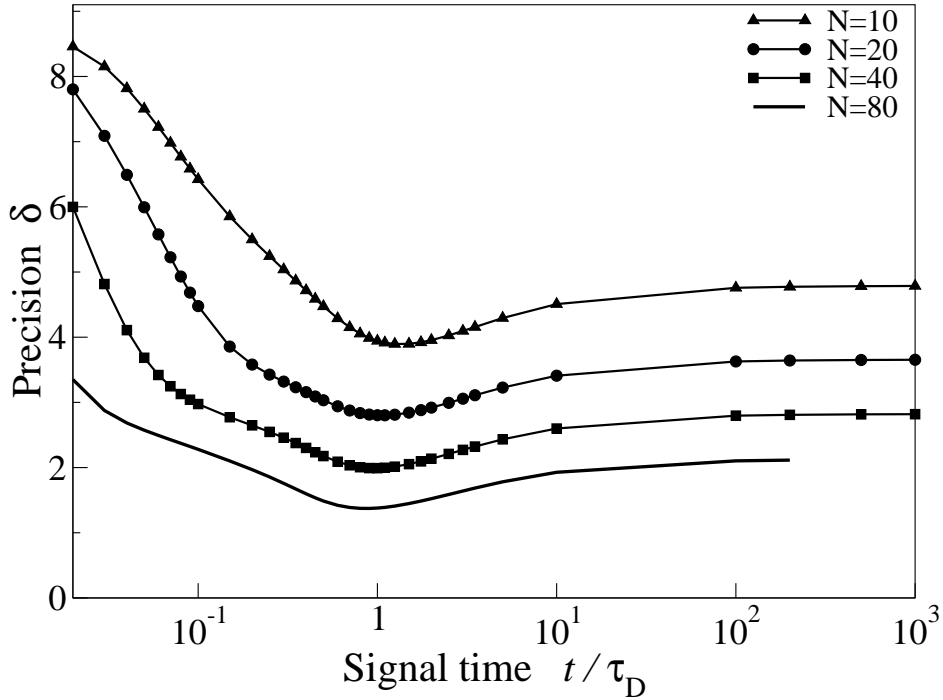
Figure 10: Spatial precision obtained for the setup of Figure 8 for the values $N = 5$, 10, 20, 40 and 80 and for record times varying from $2.10^{-2}\tau_D$ to $10^3\tau_D$. The time scale is logarithmic. A minimum of the precision is found at $t \simeq \tau_D$.

waves that reach the receiver have followed "snake-like" paths around the direct ray. For early record times, the only records sensitive to the change are those for which the change is located along the segment joining the source and the receiver. For larger record times, the diffuse waves arriving at the receiver have explored a larger volume of the system. This qualitatively explains why $\delta$ decreases with the record time $t$. At very late times, the formula (20) reveals that the decorrelation for each source receiver pair saturates, as the exponential factor tends to 1. The asymptotic spatial sensitivity to the change is algebraic only. After reaching a minimum, $\delta$ increases because the variations of $\chi_n^2$ with respect to x decreases. The minimum for $\delta$ is found approximately at time $\tau_D$, the Thouless time, after which the whole system has been explored by the diffuse waves and yet $Q$ still exhibits large spatial variations.
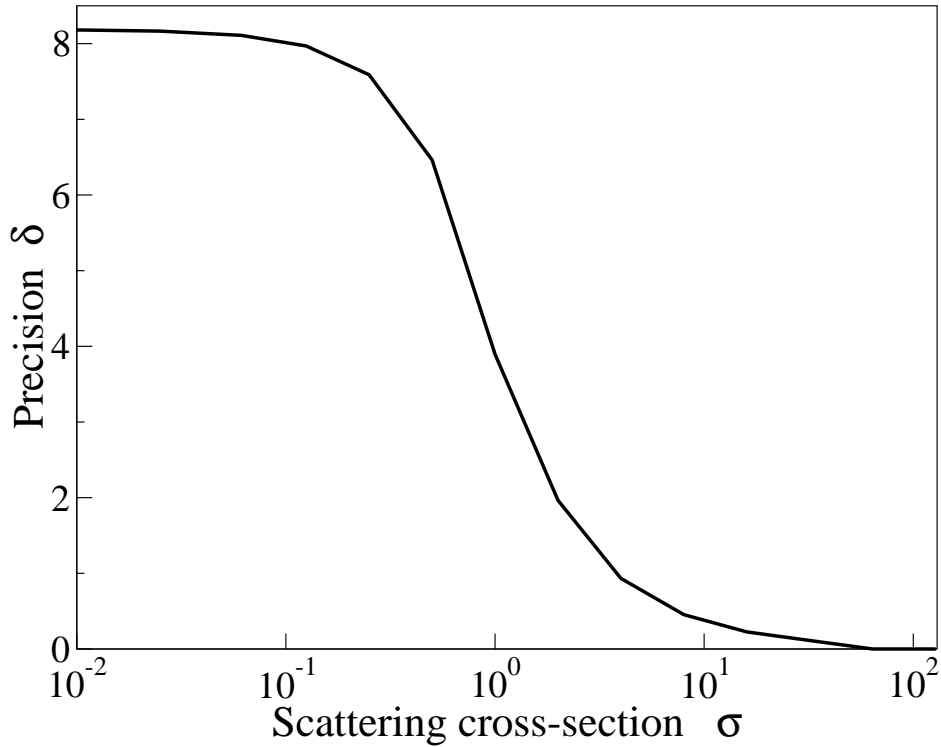
Figure 11: Optimal precision $\delta$ as a function of the cross-section of the change $\sigma$ obtained for the setup of Figure 8. Other parameters of the simulations are $D = 1$, $c = 1$, $N = 10$, $\epsilon = 0.01$.

## 4.4 Precision versus cross-section

The scattering cross-section $\sigma$ of the change also influences the precision of the technique. We observe that the precision $\delta$ decreases as $\sigma$ increases. Note that when $\sigma$ is very small, $\delta$ goes to a value $\sim L$, meaning that it is not possible to detect the change. When $\sigma \simeq L^2$, the cross-section is equivalent to the area of the system, and locating a change has no physical significance in this limit. In Figure 11 we plot the variations of $\delta$ at the optimal time $t = \tau_D$ as $\sigma$ varies from $10^{-4}L^2$ to $L^2$. The other parameters of the calculations are $D = 1$, $c = 1$, $\epsilon = 0.01$, $N = 10$. We observe that the spatial precision $\delta$ decreases by a factor 2 as the cross-section increases from $10^{-2}$ to $1$.

## 4.5 Sensitivity to the value of the diffusivity $D$

Our inversion procedure depends heavily upon our ability to estimate the diffusivity of the waves in the heterogeneous medium. Although the absorption time $\tau$ does not enter into the final formula (20), let us remark that in practice $D$ and $\tau$ cannot be measured independently. The diffusivity $D$ is the crucial physical parameter which enters into the formula for the intensity propagator $P_d$ and controls the accuracy of the energy propagation model of the medium. It is therefore important to quantify the impact of errors in the diffusivity $D$ on the accuracy of our method. Even if we use an incorrect value for the diffusivity, our inversion procedure still provides an answer for the position of the change. The main issue is to quantify to what extent the inferred position differs from the exact location of the target. To address this point, we plot the spatial precision and the absolute error of the inversion for a wide range of values of $D$ on a specific example.

We use the approach described in Section 4.2. First, a synthetic data set is computed with a value $D$ for the diffusivity. This synthetic data set is then inverted for the location of the target using a different diffusivity $D'$. The change is located at the position $\mathbf{x}_1$ indicated on Figure 8. The other physical parameters $L = 10$, $\sigma = 1$, $N = 10$, $\epsilon = 0.01$ and $t$ have been adjusted to provide the smallest spatial precision $\delta$. We call $\xi$ the distance between the change located by the inversion and $\delta$ is the spatial precision. The results of the simulation are displayed in Figure 12. It is rather remarkable that an error on $D$ as large as a factor of 2 yields a location of the change within one half of the spatial precision. In this specific but realistic example, the inversion procedure is therefore very robust against errors on the determination of $D$. This constitutes a major advantage of our method. Based on these results, we infer that spatial variations of $D$ within a factor of 2 will not affect the results dramatically.

# 5 Boundary conditions

The inversion procedure presented in section 4 relies on the knowledge of the function $P_d$, the diffusion kernel, which depends on the boundary conditions of the system. For simplicity, we studied the LOCADIFF technique in an infinite medium without taking into account the effect of boundaries, which may not be realistic in applications. An abundant literature is dedicated to solving the diffusion equation in a wide range of situations [7]. In many cases of practical interest, sophisticated techniques are required to provide an exact solution or a numerical
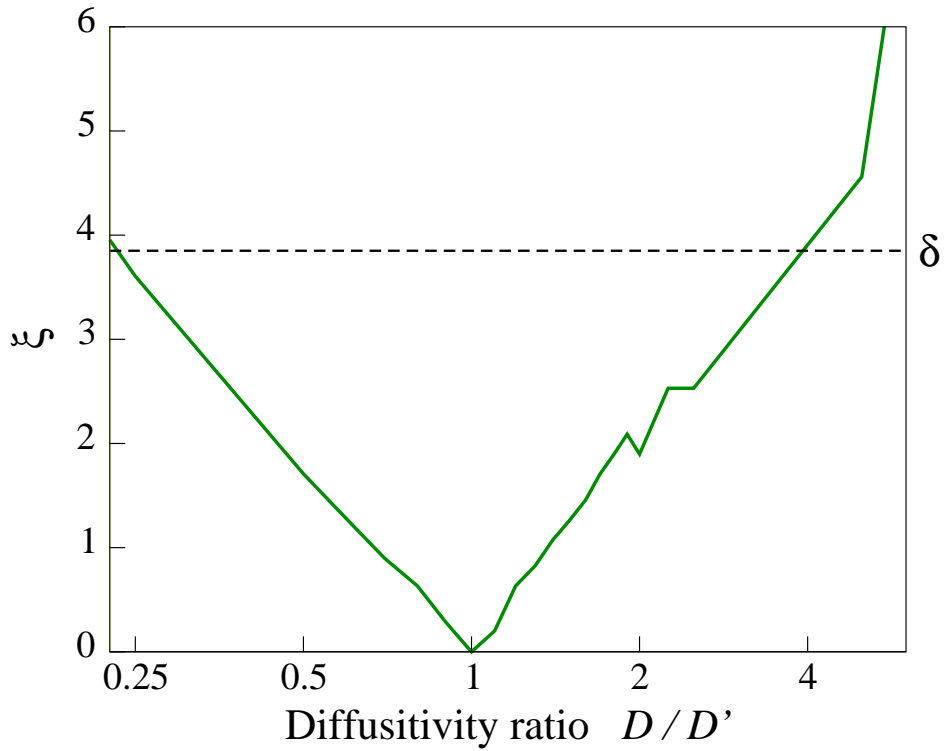
Figure 12: Effect of errors on the value of the diffusivity $D$ on the relocation accuracy of the target. Synthetic data were calculated with $D = 1$ and inverted with modified values of the diffusivity $D'$ ranging from 0.2 to 8. The other parameters of the simulation are $\sigma = 1$, $L = 10$, $N = 10$, $\epsilon = 0.01$ and the change is located at the position $\mathbf{x}_1$ (see Figure 8). $\xi$ is the distance between $\mathbf{x}_1$ and the point where $\chi^2(\mathbf{x})$ is minimum. In the simulated configuration, the inversion procedure remains accurate even if $D'$ differs from $D$ by a factor 2.

approximation up to a required accuracy. In the infinite medium, the decorrelation (18) can be computed numerically. In the presence of boundaries, it is more difficult to compute the Green's function because translational invariance is lost. However, if the boundaries are flat, it is possible to construct the Green's function from the solution without boundaries using symmetry arguments. In the general case, one has to solve the diffusion equation for the geometry of the system, which is a problem of applied mathematics in itself.

In the simple case of a single planar boundary, the solution $P_d^B$ of the diffusion equation of the semi-infinite medium, can be deduced from $P_d^\infty$, using the technique of images:

$$P_d^B(\mathbf{s},\, \mathbf{r},\, t) = \alpha \left( P_d(\mathbf{s},\, \mathbf{r},\, t) + \beta P_d(\mathbf{s}',\, \mathbf{r},\, t) \right) \tag{30}$$

where $\mathbf{s}'$ is the image of $\mathbf{s}$ with respect to the boundary (see Figure 13) and $\beta$ is a characteristic coefficient depending on the nature of the boundary condition. For instance if the boundary is absorbing, $\beta = -1$ and if it is fully reflecting, we have $\beta = 1$. The normalization coefficient $\alpha$ is, in the case of constant diffusivity

$$\alpha^{-1} = \frac{1+\beta}{2} + \frac{1-\beta}{2} \operatorname{erf}\left( \frac{d_{B,\mathbf{s}}}{\sqrt{4Dt}} \right) \tag{31}$$

where $d_{B,\mathbf{s}}$ is the distance from the source to the boundary. Note that $\alpha$ is undetermined in the case where the conditions $\beta = -1$ and $d_{B,\mathbf{s}} = 0$ are met simultaneously. The solution to the diffusion equation in presence of the boundary can be
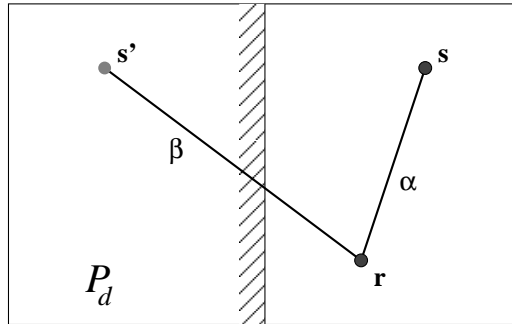


Figure 13: Schematic representation of a boundary condition for $P_d$. The image of the source $\mathbf{s}$ is noted $\mathbf{s}'$ and the arbitrary point is $\mathbf{r}$. The solid line is the solution in the infinite medium.

plugged into the decorrelation expression (18) leading to four terms (figure 14).

Note that in the case where there are more boundaries, infinitely many images must be taken into account in the formula. Other techniques also lead to infinite series.
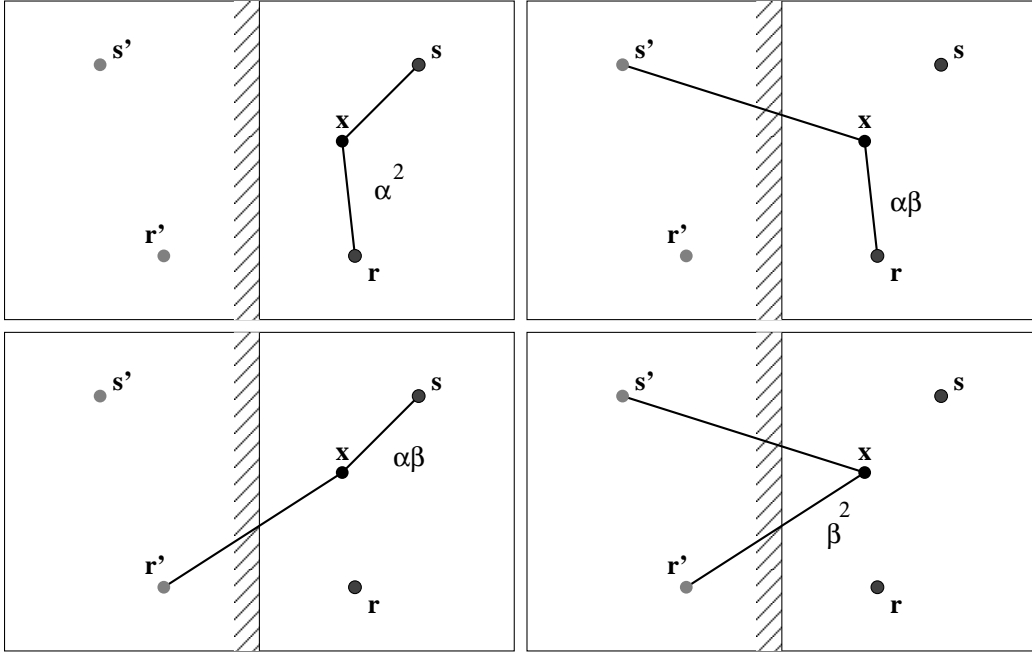


Figure 14: In presence of a single straight boundary, the decorrelation function (18) involves four terms, coming from the product of two formula of the form (30). We use the images of the source **s** and the receiver **r**: Thanks to the symmetry of the diffusion equation, there is no need to introduce the image of the point **x**.

# 6 Discussion

In this section, we discuss issues related to the practical use of the LOCADIFF technique as well as possible improvements. We first note that if the interval between the records of $h_{ij}$ and $h'_{ij}$ is large, the medium may also have experienced a global change, for instance a dilation due to a temperature change. In this case, the computation of the decorrelation may be refined by taking into account a global

26

relative velocity change $\eta$, where $\epsilon$ yields the maximum value of the correlation

$$\frac{\int h_{ij}((1+\eta)u)\, h'_{ij}(u)\mathrm{d}u}{\sqrt{\int h_{ij}(u)^2\mathrm{d}u \int h'_{ij}(u')^2\mathrm{d}u'}}. \tag{32}$$

where the integrals are performed along the whole record [13].

Another issue concerns the possible improvements on the inversion procedure. Under the form presented in this article, the LOCADIFF technique only uses a small time window in the signals, and it would be of great interest to take into account several time windows simultaneously. This would provide more independent data for the inversion procedure and may reduce the effect of noise.

Finally, we point out that the kernel used in the inversion is computed from the solution to the diffusion equation. In some simple geometries, like the infinite medium, the solution is analytic and simple to compute. If the shape of the medium is irregular, with possibly more complicated boundary conditions, the kernels can only be approximated numerically. Alternatively, our approach could benefit from recent developpements in the implementation of the radiative transfer equation.

# 7   Conclusion

In this article, we have shown that it is possible to use the high sensitivity of diffuse waves to detect, characterize and locate a weak change in a strongly scattering medium. Our technique uses the correlation of waveforms recorded before and after the change. Based on a maximum-likelihood approach, and a simple diffusion model, we demonstrate the possibility to retrieve the position of the change along with its scattering cross-section. We have also investigated the optimal values of the parameters that enter in the inversion procedure, based on a simple setup where sources and receivers are arranged on a circle surrounding the change. Three features have been identified: 1) We found that the precision scales with the inverse square root of the number of sensors. 2) The technique provides the best results when the correlation window is centered on the Thouless time of the system. 3) We demonstrated that the technique is not very sensitive to errors in the measurement of the diffusivity.

Several aspects are still to be investigated. First, we have assumed that a single change occurs in the medium, an assumption which is probably too restrictive in some applications. In a straightforward generalization of our technique to $n$

27

changes, the dimension of the parameter space scales like $4n$ which in turn considerably increases the computation time. An alternative route for the inversion has to be found. Second, we have made the assumption of a point-like change. An extended change may not necessarily be equivalent to a collection of point-like changes. Again, an alternative approach to the inverse problem will be needed. We are currently investigating these two issues.

Using 2D finite difference wave simulations, we have demonstrated that LOCADIFF efficiently locates a weak change in a multiple scattering environment. In a separate paper [15], experiments have also been conducted with ultrasound in concrete. The change was a hole drilled in the sample, and the LOCADIFF technique successfully retrieved its actual position. Other applications in geophysics and material sciences can be envisaged.

## Acknowledgments

## A    Derivation using Bayesian inversion

We shortly derive here the density of probability density (29) using a Bayesian inference. In this calculation, we suppose that there is a change at an unknown position $\mathbf{x}$. The values of the measurements $K_{ij}^m$ are accurate up to an error order $\epsilon$ such that they are distributed around the numerical value $K_{ij}(\mathbf{x}, t)$ according to a standard error function.

$$p(K_{ij}^m|\mathbf{x}) = \frac{1}{\sqrt{2\pi}\epsilon} \exp\left[-\frac{(K_{ij}(\mathbf{x},\,t) - K_{ij}^m)^2}{2\epsilon^2}\right]. \tag{33}$$

Each pair $(i, j)$ provides an independent information. The Bayesian inversion consists in finding the probability density of $\mathbf{x}$ knowing the values of $K_{ij}^m$, namely to compute $p(\mathbf{x}|\{K_{ij}^m\})$. Let us call $p_n(\mathbf{x})$ the probability density for the position of the change when $n$ source-receiver pairs have been taken into account. Before measurement, the probability of the location of the change is uniform in the whole medium, so we have $p_0(\mathbf{x}) = \frac{1}{V}$ ($V$ is the volume). Suppose we know $p_{n-1}(\mathbf{x})$ and let us compute the joint probability of $\mathbf{x}$ and $K_n$ using Bayes' formula. We

use the two relations:

$$p(\mathbf{x}, K_n^m | K_1^m, \ldots K_{n-1}^m) = p_n(\mathbf{x}) p(K_n^m) \tag{34}$$

$$p(\mathbf{x}, K_n^m | K_1^m, \ldots K_{n-1}^m) = p(K_n^m | \mathbf{x}) p_{n-1}(\mathbf{x}) \tag{35}$$

Integrating (34) over $\mathbf{x}$ we can compute $p(K_n^m)$ as

$$\left( \int_V p_n(\mathbf{x}) \mathrm{d}\mathbf{x} \right) p(K_n^m) = \int_V p(\mathbf{x}, \, K_n^m | K_1^m, \, \ldots K_{n-1}^m) \mathrm{d}\mathbf{x} \tag{36}$$

The integral of $p_n(\mathbf{x})$ is equal to $1$ so we conclude that, using (35),

$$p_n(\mathbf{x}) = \frac{p(K_n^m | \mathbf{x}) p_{n-1}(\mathbf{x})}{\int_V p(K_n^m | \mathbf{x}) p_{n-1}(\mathbf{x}) \mathrm{d}\mathbf{x}}. \tag{37}$$

Therefore we have a recurrence scheme yielding the distribution of probability $p_N(\mathbf{x})$:

$$p_N(\mathbf{x}) = \frac{\prod_{n=1}^N p(K_n^m | \mathbf{x})}{\int \prod_{n=1}^N p(K_n^m | \mathbf{x}) \mathrm{d}\mathbf{x}} \tag{38}$$

which gives Equation (29) after replacing the probabilities with expression (33).

# References

[1] E. Akkermans and G. Montambaux. *Mesoscopic physics of electrons and photons*. Cambridge Univ Press, 2007.

[2] Alexandre Aubry and Arnaud Derode. Random matrix theory applied to acoustic backscattering and imaging in complex media. *Phys. Rev. Lett.*, 102:084301, 2009.

[3] Richard Berkovits. Sensitivity of the multiple-scattering speckle pattern to the motion of a single scatterer. *Phys. Rev. B*, 43:8638–8640, 1991.

[4] F. Brenguier, M. Campillo, C. Hadziioannou, N. M. Shapiro, R. M. Nadeau, and É. Larose. Postseismic relaxation along the San Andreas fault at Parkfield from continuous seismological observations. *Science*, 321:1478–1482, 2008.

[5] M. L. Cowan, I. P. Jones, J. H. Page, and D. A. Weitz. Diffusing acoustic wave spectroscopy. *Phys. Rev. E*, 65:066605, 2002.

[6] M. L. Cowan, J. H. Page, and D. A. Weitz. Velocity fluctuations in fluidized suspensions probed by ultrasonic correlation spectroscopy. *Phys. Rev. Lett.*, 85:453–456, 2000.

[7] J. Crank. *The mathematics of diffusion*. Oxford, 2nd edition, 1975.

[8] P. N. den Outer, Th. M. Nieuwenhuizen, and Ad Lagendijk. Location of objects in multiple-scattering media. *J. Opt. Soc. Am. A*, 10:1209–1218, 1993.

[9] Arnaud Derode, Éric Larose, Mickaël Tanter, Julien de Rosny, Arnaud Tourin, Michel Campillo, and Mathias Fink. Recovering the Green's function from field-field correlations in an open scattering medium. *J. Acoust. Soc. Am.*, 113:2973–2976, 2003.

[10] E. N. Economou. *Green's Functions in Quantum Physics*. Springer, Berlin, 2006.

[11] Sechao Feng and Didier Sornette. Acoustical nondestructive evaluation of heterogeneous materials in the multiple scattering regime. *J. Acoust. Soc. Am.*, 90:1742–1748, 1991.

[12] P. Gouédard, L. Stehly, F. Brenguier, M. Campillo, Y.C. de Verdiere, E. Larose, L. Margerin, P. Roux, FJ Sanchez-Sesma, Shapiro NM, and RL Weaver. Cross-correlation of random fields: mathematical approach and applications. *Geophysical prospecting*, 56(3):375–393, 2008.

[13] Éric Larose and Stephen Hall. Monitoring stress related velocity variation in concrete with a $2.10^{-5}$ relative resolution using diffuse ultrasound. *J. Acoust. Soc. Am.*, 125:1853–1856, 2008.

[14] Éric Larose, Ludovic Margerin, Arnaud Derode, Bart van Tiggelen, Michel Campillo, Nikolai Shapiro, Anne Paul, Laurent Stehly, and Mickaël Tanter. Correlation of random wavefields: An interdisciplinary review. *Geophysics*, 71:SI11–SI21, 2006.

[15] Éric Larose, Thomas Planès, Vincent Rossetto, and Ludovic Margerin. Locating a small change in a multiple scattering environment. *Appl. Phys. Lett.*, 96:204101, 2010.

[16] Oleg I. Lobkis and Richard L. Weaver. Coda-wave interferometry in finite solids: recovery of P-to-S conversion rates in an elastodynamic billiard. *Phys. Rev. Lett.*, 90:254302, 2003.

[17] Jennifer E. Michaels and Thomas E. Michaels. Detection of structural damage from the local temporal coherence of diffuse ultrasonic signals. *IEEE Trans. Ultrasonics, Ferroelectrics and Freq. Control*, 52:1769–1782, 2005.

[18] Th. M. Nieuwenhuizen and van Rossum M. C. W. Rôle of a single scatterer in a multiple scattering medium. *Physica A*, 177:102–106, 1993.

[19] Carlos Pacheco and Roel Snieder. Time-lapse travel time change of multiply scattered acoustic waves. *J. Acoust. Soc. Am.*, 118:1300–1310, 2005.

[20] David J. Pine, D. A. Weitz, P. M. Chaikin, and E. Herbolzheimer. Diffusing-wave spectroscopy. *Phys. Rev. Lett.*, 60:1134–1137, 1988.

[21] G. Poupinet, WL Ellsworth, and J. Frechet. Monitoring velocity variations in the crust using earthquake doublets: an application to the Calaveras fault, California. *J. Geophys. Res*, 89(B7):5719–5731, 1984.

[22] G. Poupinet, J.-L. Got, and F. Brenguier. *Earth Heterogeneity and Scattering Effects on Seismic Waves*, volume 50 of *Advances in Geophysics*, chapter Monitoring temporal variations of physical properties in the crust by cross-correlating the waveforms of seismic doublets, pages 374–399. Academic Press, New York, 2008.

[23] A. Ratdomopurbo and G. Poupinet. Monitoring a temporal change of seismic velocity in a volcano: Application to the 1992 eruption of Mt. Merapi (Indonesia). *Geophys. Res. Lett*, 22(7):775–778, 1995.

[24] Peter M. Roberts, W. Scott Phillips, and Michael C. Fehler. Development of the active doublet method for measuring small velocity and attenuation changes in solids. *J. Acoust. Soc. Am.*, 91:3291–3302, 1992.

[25] Christoph Sens-Schönfelder and U. Wegler. Passive image interferometry and seasonal variations of seismic velocities at Merapi volcano, Indonesia. *Geophys. Res. Lett.*, 33:L21302, 2006.

[26] P. Sheng. *Introduction to wave scattering localization and mesoscopic phenomena*. Springer, Berlin, 2006.

[27] R. Snieder and J. Page. Multiple scattering in evolving media. *Physics today*, 60(5):49–55, 2007.

[28] Roel Snieder, Alexandre Grêt, Huub Douma, and John Scales. Coda wave interferometry for estimating nonlinear behavior in seismic velocity. *Science*, 295:2253–2255, 2002.

[29] N. Tremblay, Éric Larose, and Vincent Rossetto. Slow dynamics of porous multicomposite material probed by diffuse acoustic wave spectroscopy. *J. Acoust. Soc. Am.*, 127:1239–1243, 2010.

[30] M. C. W. van Rossum and Th. M. Nieuwenhuizen. Multiple scattering of classical waves: miscroscopy, mesoscopy and diffusion. *Rev. Mod. Phys.*, 71:313–371, 1999.

[31] Christian Vanneste, Sechao Feng, and Didier Sornette. Non-destructive evaluations in multiple-scattering media. *Europhys. Lett.*, 24:339–344, 1993.

[32] K. Wapenaar, J. Fokkema, and R. Snieder. Retrieving the Green's function in an open system by cross correlation: A comparison of approaches (L). *J. Acoust. Soc. of Am.*, 118:2783–2786, 2005.

[33] K. Wapenaar, E. Slob, and R. Snieder. Unified Green's function retrieval by cross correlation. *Phys. Rev. Lett.*, 97(23):234301, 2006.

[34] Ulrich Wegler and C. Sens-Schönfelder. Fault zone monitoring with passive image interferometry. *Geophys. J. Int.*, 168:1029–1033, 2007.